RSC Advances

PAPER

View Article Online
View Journal | View Issue

Cite this: *RSC Adv.*, 2015, **5**, 40521

Robust electrospinning cellulose acetate@TiO_2 ultrafine fibers for dyeing water treatment by photocatalytic reactions

Shu-Dong Wang,†*[ab] Qian Ma,†[b] Hua Liu,*[b] Ke Wang,[b] Liang-Zhong Ling[c] and Ke-Qin Zhang*[a]

Cellulose acetate (CA) composite ultrafine fibers containing different TiO_2 nanoparticle (NP) contents were synthesized *via* electrospinning for effective dyeing water treatment. Morphology, chemical composition, microstructure, thermal properties and photocatalytic degradation efficiency of the fabricated composite ultrafine fibers were investigated. Scanning Electron Microscopy (SEM) and Transmission Electron Microscopy (TEM) images revealed that TiO_2 NPs were evenly dispersed on or into the composite ultrafine fibers and the distribution became denser as the concentration of TiO_2 NPs increased. This was also confirmed by Energy Dispersive Spectrometry (EDS), X-ray diffraction (XRD) and Fourier Transform Infrared Spectrometry (FTIR) analyses. Moreover, the results of XRD showed that the crystal structure of the TiO_2 NPs was tetragonal anatase and the TiO_2 NPs enhanced the amorphous phase of the electrospun composite ultrafine fibers. FTIR indicated that the introduction of TiO_2 did not affect the hydrophilic properties of CA and some interaction took place between CA and TiO_2. Thermal gravimetric (TG) analysis showed that the addition of TiO_2 improved the thermal stability of the CA ultrafine fibers, and a higher thermal stability could be achieved with a higher TiO_2 content. Photocatalytic degradation of the dye showed that a higher reaction constant of the photocatalytic degradation of the dye could be obtained with a higher TiO_2 content, with a degradation efficiency of the CA composite ultrafine fibers with 5 wt% TiO_2 as high as 90% after 240 min degradation. The composite ultrafine fibers were effective for cycling use in dyeing water treatment.

Received 3rd March 2015
Accepted 13th April 2015

DOI: 10.1039/c5ra03797b

www.rsc.org/advances

Dye waste water generated from the textile industry has been considered as one of the major sources of water pollution due to the high consumption of water in dyeing, printing and finishing processes. About 20% of the dye is lost in the dyeing process and is released in the waste water.[1] Generally, waste water produced from this industry is complex in composition and variable in nature, highly colored and contaminated, contains a high level of organic products and hard to be biodegraded. Beside the aesthetically undesirable appearance, most dyes may adversely affect ecosystem and may pose potential carcinogenic and mutagenic risk to humans and aquatic organisms.[2–4] Commonly technologies used for dye removal include physical, chemical, biological methods or various combinations of them. However, these methods are proved to be either inefficient or cost effective, some even generate secondary.[5,6] For this reason, photocatalytic process has been proposed as one useful method to decolorize waste water in recent years because the semiconductor photocatalysts it involved can function effectively at mild condition and very low concentration to completely minimize the environmental hazard.[7] Among the various semiconductor photocatalysts, TiO_2 (especially in anatase phase) is believed to be the best for water treatment because of its high photoactivity, non-toxicity, stability, mechanical robustness, low cost, and proven ability to convert effectively carbon from organic compounds to carbon dioxide.[8,9] However, the major problem of TiO_2 stem from its significant drawbacks such as difficult removal from solution for cycling use, tendency of agglomeration and do harm to living organisms with exposure in environment.[10,11]

In order to solve this problem, great attention has been focused on incorporating TiO_2 NPs into some polymer carriers by means of nanotechnologies, such as self-assembly, phase separation, sol–gel, and electrospinning. During these fabrications, electrospinning has been paid much attention to because it can prepare three-dimensional nano-scale nonwoven mats

[a]*National Engineering Laboratory for Modern Silk, College of Textile and Clothing Engineering, Soochow University, Suzhou 215123, P. R. China. E-mail: sdwang1983@163.com; kqzhang@suda.edu.cn*

[b]*Jiangsu Research and Development Center of the Ecological Textile Engineering and Technology, College of Textile and Clothing, Yancheng Institute of Industry Technology, Yancheng 224005, P. R. China. E-mail: sdwang1983@163.com; ycfylh@126.com*

[c]*Jiangsu Yueda Nanwei Textile Technologies Limited Company, Yancheng 224007, P. R. China*

† These authors contributed equally to this publication.

with an extremely large surface-to-volume and high porosity. Moreover, the composition and structure can be controlled to achieve desired properties and functionality. The electrospinning ultrafine fibers, which not also combine the photocatalytic function of TiO_2 and the nanofiltration function, but also better exhibit the photocatalytic function of TiO_2 due to the increasing surface-area-to-volume ratio may provide a sufficient area for interaction without agglomeration of NPs. Moreover, reuse of TiO_2 can be achieved as the electrospinning nonwoven mats as carriers.[11,12] To date, there are some reports about electrospinning nonwoven mats incorporating TiO_2 NPs for water treatment using some polymer carriers, such as PAN, nylon-6, PVA, and so on.[13–17] However, all issues with these membranes are their hydrophobicity which leads to severe membrane fouling and decline of permeability.[18] Although high fouling tendency of these membranes can be reduced by changing forming method, their porous structure disappears as well.[19] Among all the polymers, cellulose and its derivatives are considered of significant industrial importance with some prominent advantages such as low cost, biodegradability, good mechanical properties, nontoxicity, and high stability to most organic solvents.[20] Moreover, they have high density of hydroxyl groups which will make them less prone to organic fouling.[18] So far, few studies are available on utilization of the natural antifouling property and the photoactivity of the TiO_2/cellulose nanocomposite.

Therefore, the focus of this work is to prepare CA composite membranes with TiO_2 NPs using electrospinning of blend of these materials for dyeing water treatment. In order to obtain better dispersion of TiO_2 in CA solution, ultrasonic irradiation was employed. Aqueous methyl blue (MB) was used to test photocatalytic activity of membranes with different TiO_2 contents. Macro–micro structures and physicochemical properties of the electrospinning CA/TiO_2 ultrafine fibers were analyzed by SEM, TEM, EDS, XRD, FTIR and TG. The photocatalytic degradation efficiency of the fabricated composite ultrafine fibers was investigated. The test results show that the CA/TiO_2 nonwoven mats are appropriate candidates for dye waste water treatment.

Experimental

Materials

Cellulose acetate (CA) (M_n = 30 000, 39.8 wt% acetyl content, Sigma Aldrich), and TiO_2 NPs (purity > 99 wt%, Nanjing XFNANO Materials Tech Co., Ltd., China) were used without further purification. Acetic acid (98 wt%), acetone (98 wt%) and MB were purchased from Shanghai Chemical Reagent Co. Ltd. and used without further purification.

Preparation of electrospinning composite ultrafine fibers

Pure CA solution was prepared by dissolving 14.5 wt% CA in acetone/acetic acid (2/1, w/w) solvent system and stirring for 3 h using magnetic stirrer. TiO_2 NPs at different content (0, 1, 3 and 5 wt%) were added into the CA solution. Then, blend solutions were placed under sonication for 4 h. Electrospinning was carried out at an applied voltage of 17.5 kV, tip-to-collector distance of 15 cm, and a solution feed rate of 1 mL h^{-1} at room temperature. The ambient temperature and humidity were controlled around 23 °C and 70%. The experimental process is illustrated in Fig. 1.

Characterization of electrospinning composite ultrafine fibers

Morphologies of the ultrafine fibers were analyzed by SEM (S-4700, Hitachi) and TEM (H-7650, Hitachi). Samples for SEM were coated with gold and examined at an accelerating voltage of 15 kV. TEM samples for ultrafine fibers were prepared by electrospinning directly on a copper grid mesh coated with carbon for 15 s. Average fiber diameter and its distribution were obtained by analyzing SEM images using an image analysis program (Adobe Photoshop 7.0). Distribution of TiO_2 in the fibers was studied by EDS (S-3700N, Hitachi). Crystal structure of TiO_2 were verified by XRD (model D/max-IIB, Rigaku) with Cu Kα radiation (λ = 1.5418 Å). PeakFit 4.12 software was used to deconvolve the XRD spectra by Gaussian functions, which were integrated to evaluate the crystallinity by:

$$\text{Crystallinity}(\%) = \frac{\sum I_c}{\sum I_c + \sum I_a} \quad (1)$$

where I_c is the integrated intensity of crystal regions, I_a is the integrated intensity of amorphous regions. Identification of chemical species on ultrafine fibers was carried out by FTIR (Nicolet 5700, PE Co., USA) in the range of 400–4000 cm^{-1} with a signal resolution of 1 cm^{-1} and a minimum of 16 scans, the powdered electrospinning mats were pressed into potassium bromide (KBr) pellets before testing. Deionized water was employed as the source for the contact angle measurement. The wetting properties of water droplets on the sample surfaces were

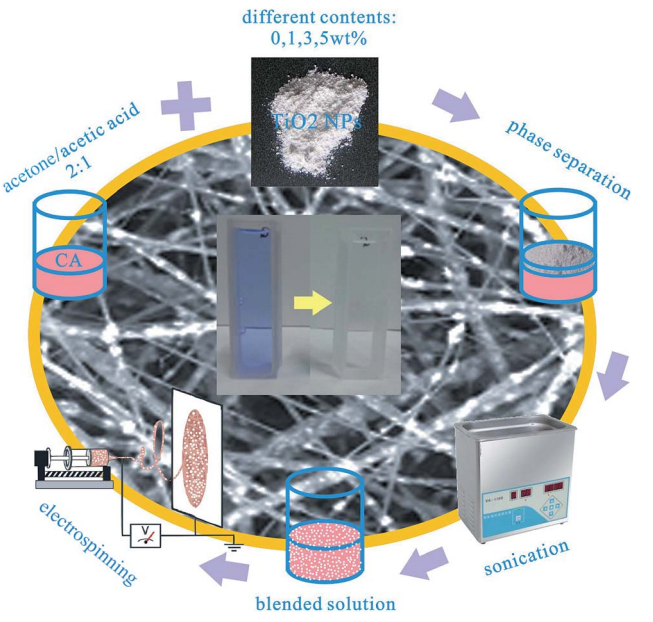

Fig. 1 Schematic illustration of the process for preparing CA composite ultrafine fibers with different TiO_2 contents.

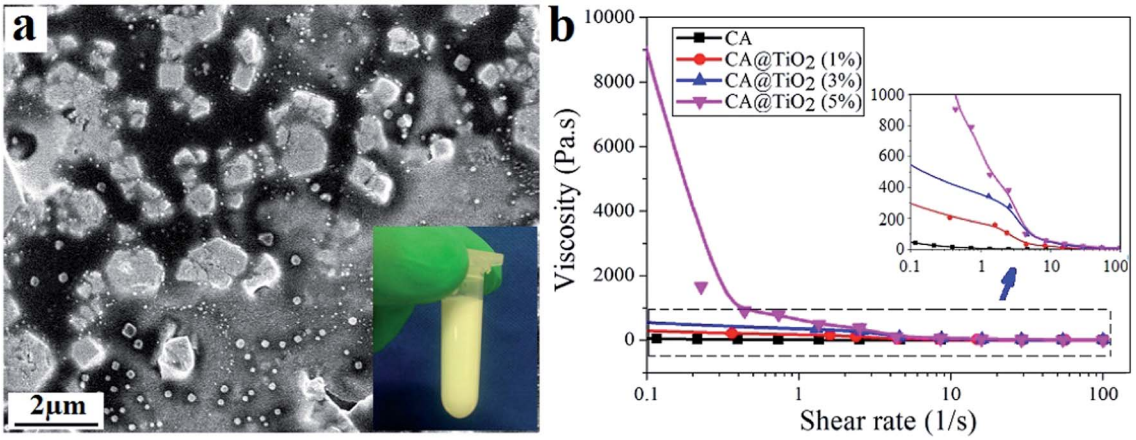

Fig. 2 Dispersion of TiO_2 NPs (a) in blended solution and viscosity (b) of the blended solution.

characterized using an optical contact-angle meter system (Krüss DSA100, Germany). The volume of droplet used for the contact angle was 6 μL. Thermal properties of the samples were investigated by a thermal analyzer (Diamond 5700, PE Co., Ltd., USA) at a heating rate of 10 °C min^{-1}, temperature range of 40–400 °C and nitrogen gas flow rate of 120 mL min^{-1}. TG curves were determined to characterize thermal stability of the ultrafine fibers.

Photocatalytic measurements

For photocatalytic activity, a 300 W mercury lamp was used as the simulated UV source. Photocatalytic capacity of as-prepared ultrafine fibers was evaluated using aqueous MB solution. Composite nonwoven mats containing different TiO_2 contents (0, 1, 3 and 5 wt%) with the same size (3 cm × 3 cm) were placed into a MB aqueous solution (10 mL, 10 mg L^{-1}). Before light irradiation, the samples were immersed with MB aqueous solution in quartz reactor at room temperature for 1 h to establish adsorption equilibrium. The reactor was equipped with a water quartz jacket to control the reaction temperature. Samples were taken at regular intervals of time (60 min), and the concentration of the dye was measured by recording its absorbance at 627 nm with a UV-visible spectrophotometer (Shimadzu UV2450, Japan).

Results and discussion

Fig. 2a showed the TiO_2 NPs had been well dispersed in the blended spinning solution after 4 h sonication, even though

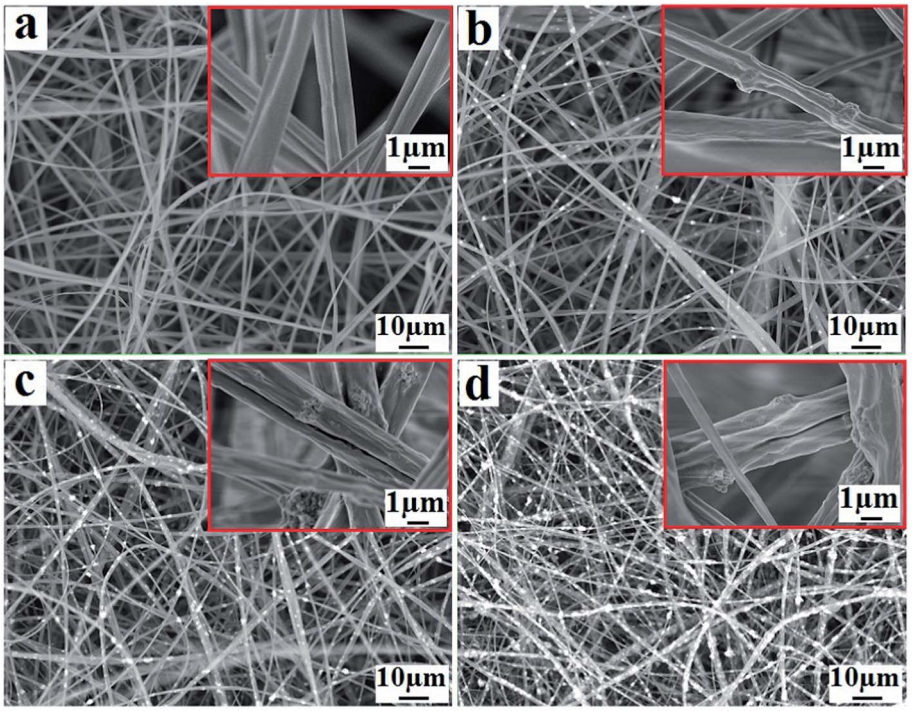

Fig. 3 SEM images of the electrospinning CA/TiO_2 composite ultrafine fibers with various TiO_2 contents: (a) 0 wt%, (b) 1 wt%, (c) 3 wt%, (d) 5 wt%.

some agglomeration occurred. Fig. 2b showed that the addition of TiO_2 NPs increased the viscosity of the solution, and this increase was more pronounced in solution containing 5 wt% TiO_2 NPs. This could be attributed to the increased concentration of the solution caused by the addition of TiO_2 NPs. SEM images of the ultrafine fibers with different TiO_2 contents were shown in Fig. 3, which indicated that beadless fibers were prepared under appropriate conditions and with moderate incorporation amount of TiO_2 NPs. As Fig. 3a showed, pure CA ultrafine fibers showed uniform, smooth and beadles fibers. With the addition of TiO_2 NPs, TiO_2 NPs could be clearly observed to be deposited on/in the ultrafine fibers evenly and its presence was denser as its concentration increased (Fig. 3b–d). However, TiO_2 NPs were agglomerated to some extent as the concentration increased due to various factors such as the charge density/potential of the powder surfaces and van der Waals forces.[21] Seen from Fig. 4, pure CA ultrafine fibers had an average diameter of 1251 ± 316 nm. As the concentration of TiO_2 increased from 0 to 5 wt%, the average fiber diameter increased gradually from 1251 ± 316 to 1437 ± 410 nm. The increase in fiber diameter could be attributed to the increase in the viscosity of the electrospinning solution when nanoparticles were incorporated as also observed in other studies,[14] which can be proved by Fig. 2. Distribution of TiO_2 on/in the fibers was also confirmed by EDS analysis (Fig. 5). As could be seen from the mapping-scan of Fig. 5b–d, a homogeneous dispersion of TiO_2 on/in the ultrafine fibers was observed and that became denser as the concentration of TiO_2 NPs increased. The atomic percentage of Ti increased from 0.96 wt% to 6.29 wt%. Besides, compared with EDS spectrum for pure CA in Fig. 5a, Fig. 5b–d also showed that TiO_2 NPs were well introduced and characteristic Ti Kα at 4.51 keV (ref. 22) were stronger with the increasing presence of TiO_2.

The internal morphology and the dispersion of TiO_2 NPs on or into the fibers were further investigated by TEM, presented in Fig. 6. We can draw the same conclusion as the SEM and EDS analysis that the incorporation percentage of TiO_2 NPs on or into the ultrafine fibers increased as the concentration increased.

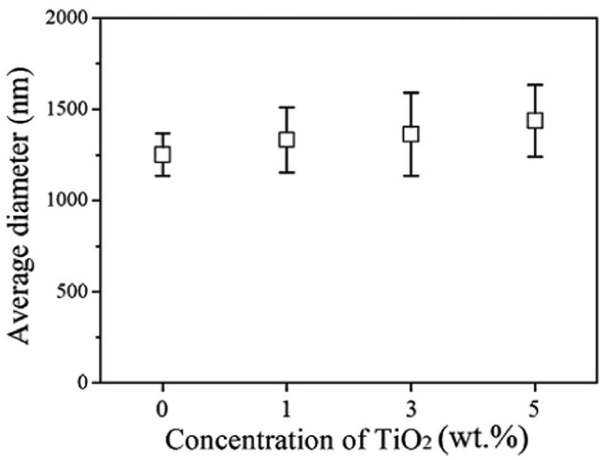

Fig. 4 Diameter distribution of the electrospinning CA@TiO_2 ultrafine fibers with different TiO_2 content.

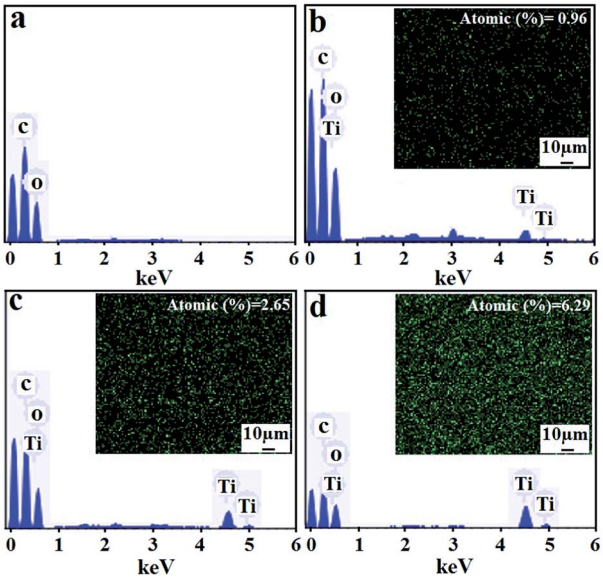

Fig. 5 EDS spectrum and distribution of titanium element of the electrospinning CA/TiO_2 composite ultrafine fibers with various TiO_2 contents: 0 wt% (a), 1 wt% (b), 3 wt% (c), 5 wt% (d).

However, agglomeration also occurred as the content of TiO_2 NPs increased. This is due to that it is easier to get aggregated if the NP content is too high. Meanwhile, it is known that TiO_2 is easy to form agglomerates because of its extremely large surface area which provides a tremendous driving force for particle bonding.[19] But this condition can be improved with a longer sonication.[9]

Fig. 7 showed the XRD patterns of CA/TiO_2 composite ultrafine fibers with various TiO_2 contents. As seen in Fig. 6a,

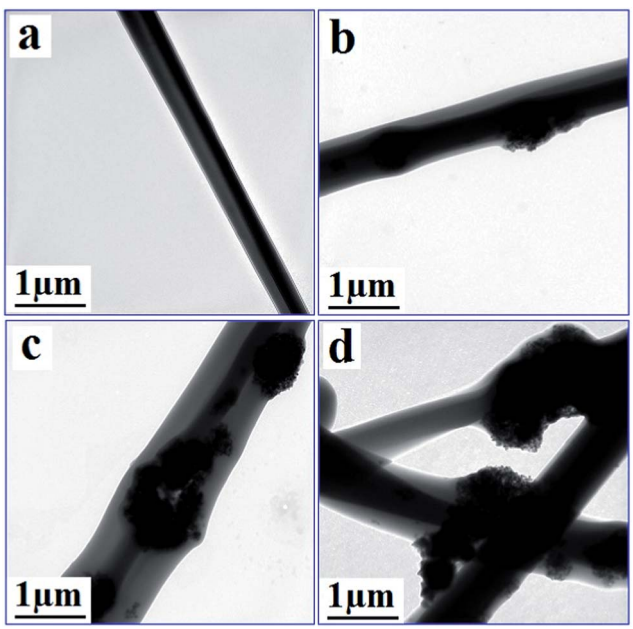

Fig. 6 TEM images of the electrospinning CA/TiO_2 composite ultrafine fibers with various TiO_2 contents: 0 wt% (a), 1 wt% (b), 3 wt% (c), 5 wt% (d).

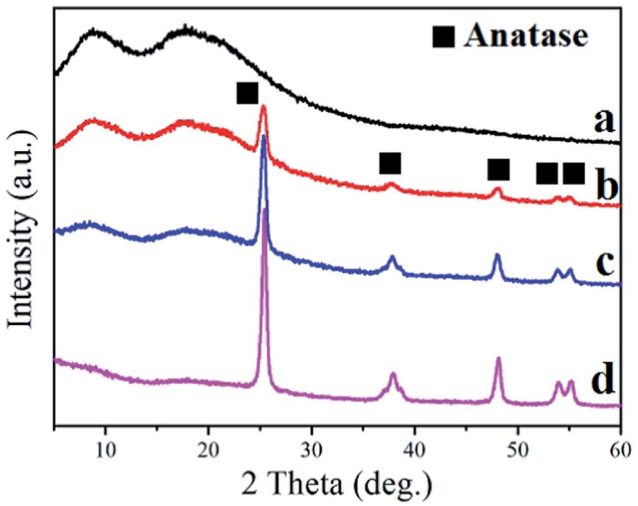

Fig. 7 XRD spectrum of the electrospinning CA/TiO_2 composite ultrafine fibers with various TiO_2 contents: 0 wt% (a), 1 wt% (b), 3 wt% (c), 5 wt% (d).

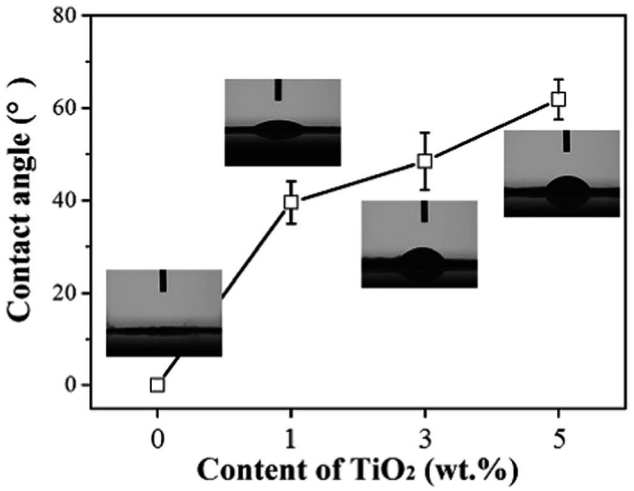

Fig. 9 Contact angle of the electrospinning CA/TiO_2 composite ultrafine fibers with various TiO_2 content.

the broad peaks appeared below $2\theta = 20°$ in the pure CA ultrafine fibers, corresponding to the semicrystalline structure of CA nonwoven mats.[23] XRD pattern of the composite nonwoven mats (Fig. 7b–d) exhibited new reflection peaks at $2\theta = 25.3°$, 37.8°, 48°, 54° and 55.09°, which were attributed to TiO_2 phase with tetragonal anatase structure.[22,24] As a result, TiO_2 NPs were successfully incorporated into the ultrafine fibers. Most important is that the anatase structure is more conducive to the photocatalysis than that of the rutile structure. The peak intensities of the crystalline anatase TiO_2 were lower than those of the semicrystalline CA due to the small amount of TiO_2 in the composite ultrafine fibers. Besides, as can be seen from Fig. 7b–d, the peak intensity belong to CA component of the composite ultrafine fibers were gradually getting weaker and even disappear while those of TiO_2 gradually getting stronger as content of TiO_2 NPs increased, revealing that the addition of TiO_2 NPs enhanced the amorphous phase of the electrospinning composite ultrafine fibers. This can be explained that the existence of TiO_2 NPs hinders the generation of crystal lattice and lead to the decrease of CA crystallinity.

To better understand interaction between TiO_2 and CA during sample preparation, we further evaluated the mats through FTIR and the spectra were shown in Fig. 8. It can be seen that all the samples showed the characteristic peaks of CA at 3500 cm^{-1} for –OH, 2960 cm^{-1} for –C–H, 1750 cm^{-1} for >C–O and 1250 cm^{-1} and 1040 cm^{-1} for –C–O– respectively.[25] Seen from Fig. 8b–d, after the incorporation of TiO_2 NPs, the intensity of peaks for –OH at 3500 cm^{-1} and –C–H at 2960 cm^{-1} remained same, while those for >C–O at 1750 cm^{-1} and –C–O– at 1250 cm^{-1} and 1040 cm^{-1} obviously were stronger as the content of TiO_2 increased, which revealed that the introduction

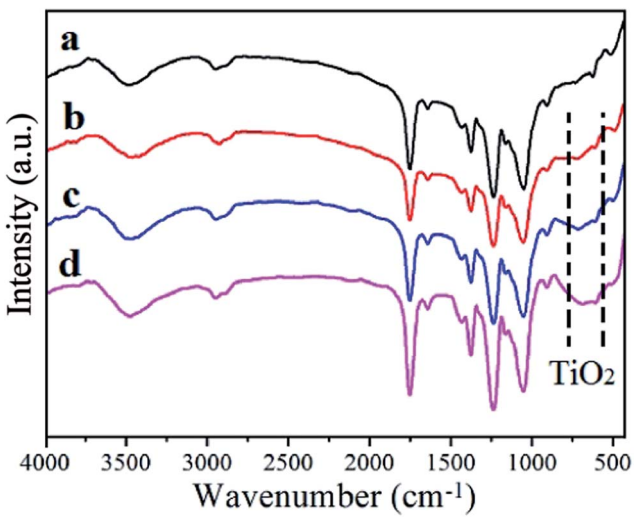

Fig. 8 FTIR spectrum of the electrospinning CA/TiO_2 composite ultrafine fibers with various TiO_2 contents: 0 wt% (a), 1 wt% (b), 3 wt% (c), 5 wt% (d).

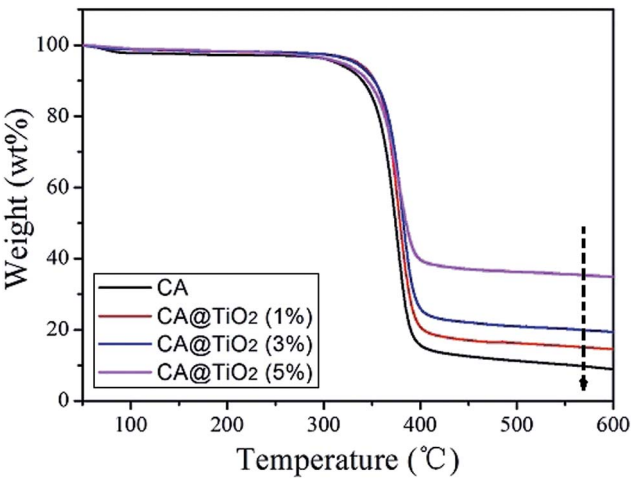

Fig. 10 TG graphs of electrospinning CA/TiO_2 composite ultrafine fibers with various TiO_2 contents: 0 wt% (a), 1 wt% (b), 3 wt% (c), 5 wt% (d).

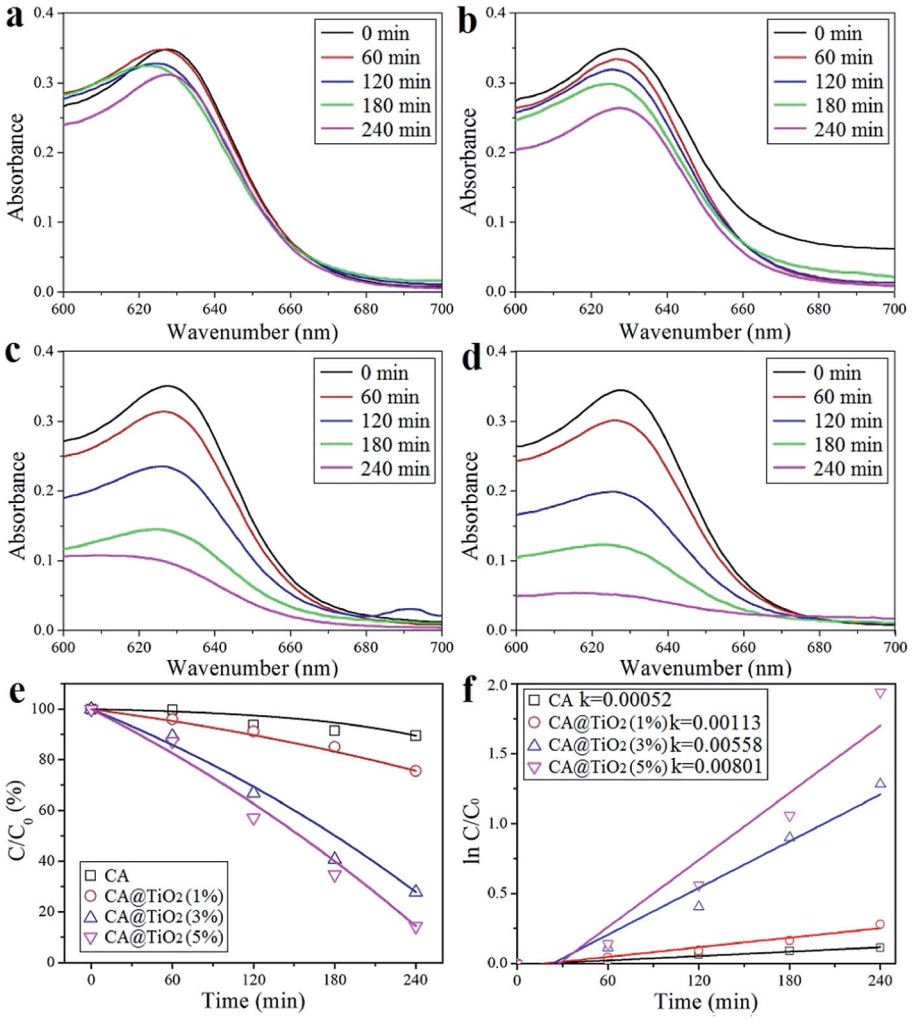

Fig. 11 UV-visible spectra of electrospinning CA/TiO_2 composite ultrafine fibers with various TiO_2 contents: 0 wt% (a), 1 wt% (b), 3 wt% (c), 5 wt% (d), reduction rates (C/C_0) (e) of MB under the composite CA ultrafine fibers with different TiO_2 contents, and photocatalytic degradation kinetics ($\ln(C/C_0)$) (f) of MB under the composite CA ultrafine fibers with different TiO_2 contents.

of TiO_2 did not affect the hydrophilic property of CA, and new >C–O and –C–O– formed between TiO_2 and CA.[26] The hydrophilic property of the ultrafine fibers could be proved by the contact angle (Fig. 9). As shown in Fig. 9, the water droplet quickly spread and wetted the pure CA ultrafine fibers were observed, indicating the CA ultrafine fibers were hydrophilic. With the introduction of TiO_2, the contact angle of the composite ultrafine fibers increased, and when the concentration of TiO_2 increases to 5 wt%, the contact angle increased to 61.9 ± 4.3°. Although the contact angle increases, the composite ultrafine fibers were still hydrophilic. Additionally, the broad peak at 569 cm^{-1} ranging from 400 cm^{-1} to 1000 cm^{-1} was the characteristic peak of neat TiO_2 NPs, which is assigned to the vibration of Ti–O.[27] It verified that anatase TiO_2 NPs have been successfully incorporated into composite ultrafine fibers. Furthermore, it can be seen that with increasing TiO_2 percentage in the composition, the specific peaks of TiO_2 between 400 cm^{-1} to 1000 cm^{-1} were more intensive.

Thermal stability of electrospinning composite ultrafine fibers was evaluated by TG. Fig. 10 showed the TG curves of CA/TiO_2 composite ultrafine fibers with various TiO_2 contents. For the pure CA ultrafine fibers, the initial decomposition temperature was 275 °C, which was lower than that of CA/TiO_2 composite ultrafine fibers. It indirectly confirmed the successful incorporation of TiO_2 NPs. From the curves, it can be noted that the composite ultrafine fibers displayed single-stage degradation, which showed the better thermal stability of composite ultrafine fibers. The decomposition temperature of composite ultrafine fibers containing 5 wt% TiO_2 was lower when compared with CA composite ultrafine fibers containing 1 and 3 wt% TiO_2, this was due to the greater amount of TiO_2 NPs in composite ultrafine fibers caused a greater reduction in the crystallinity of CA. This could be proved by the crystallinity of the electrospinning membranes. The crystallinity of pure CA is 34.5%, and overall crystallinity of composite electrospinning membranes with TiO_2 of 1, 3 and 5 wt% is 39.7%, 44.5% and 49.1% respectively. However, the ratio of crystallinity of the CA

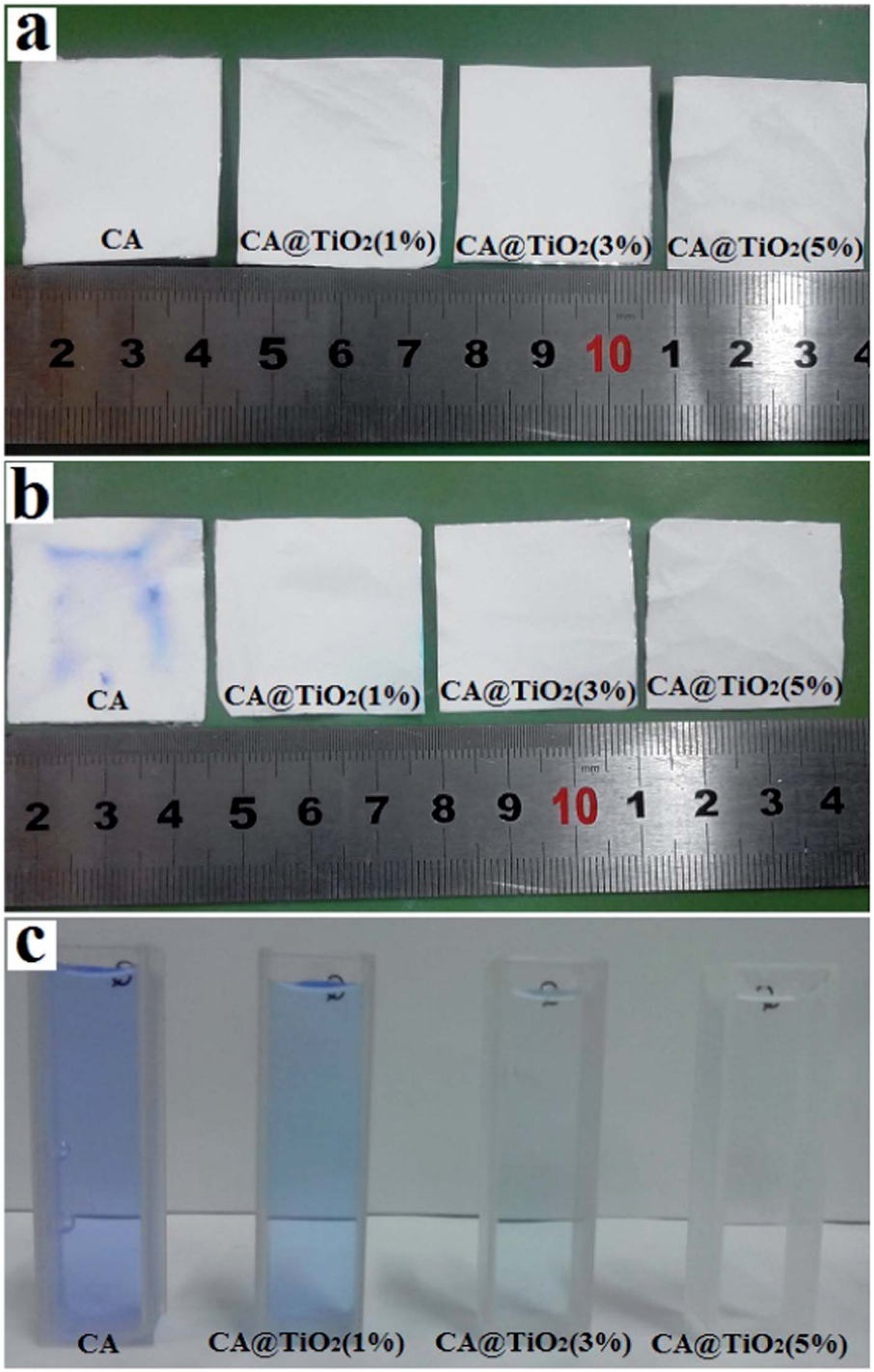

Fig. 12 Photographs of CA ultrafine fibers with different TiO_2 contents before (a) and after (b) used for MB degradation, and color change of MB under CA ultrafine fibers with different TiO_2 contents after 240 min degradation (c).

in the composite electrospinning membranes with TiO_2 of 1, 3 and 5 wt% is 28.2%, 16.5% and 3.2% respectively. Nevertheless, weight loss of composite ultrafine fibers containing 5 wt% TiO_2 was still the least, with the percentage were about 90%, 85%, 80%, 60% respectively for 0, 1, 3, 5 wt% TiO_2 content. Obviously, the addition of TiO_2 improved the thermal stability of CA ultrafine fibers, and residual weight of the composite increased with the increase of TiO_2 content. Due to the temperature of the dye waste water is high, the thermal stability of the CA/TiO_2 nonwoven mats is fit for the high temperature.

Catalytic activity of the CA composite ultrafine fibers with different TiO_2 contents was compared by the photocatalytic degradation of MB dye under the irradiation of UV lights. As shown in Fig. 11a–d, the intensity of the absorption for all samples decreased to various extents as the degradation of MB. But the intensity of the absorption for all samples at 627 nm was

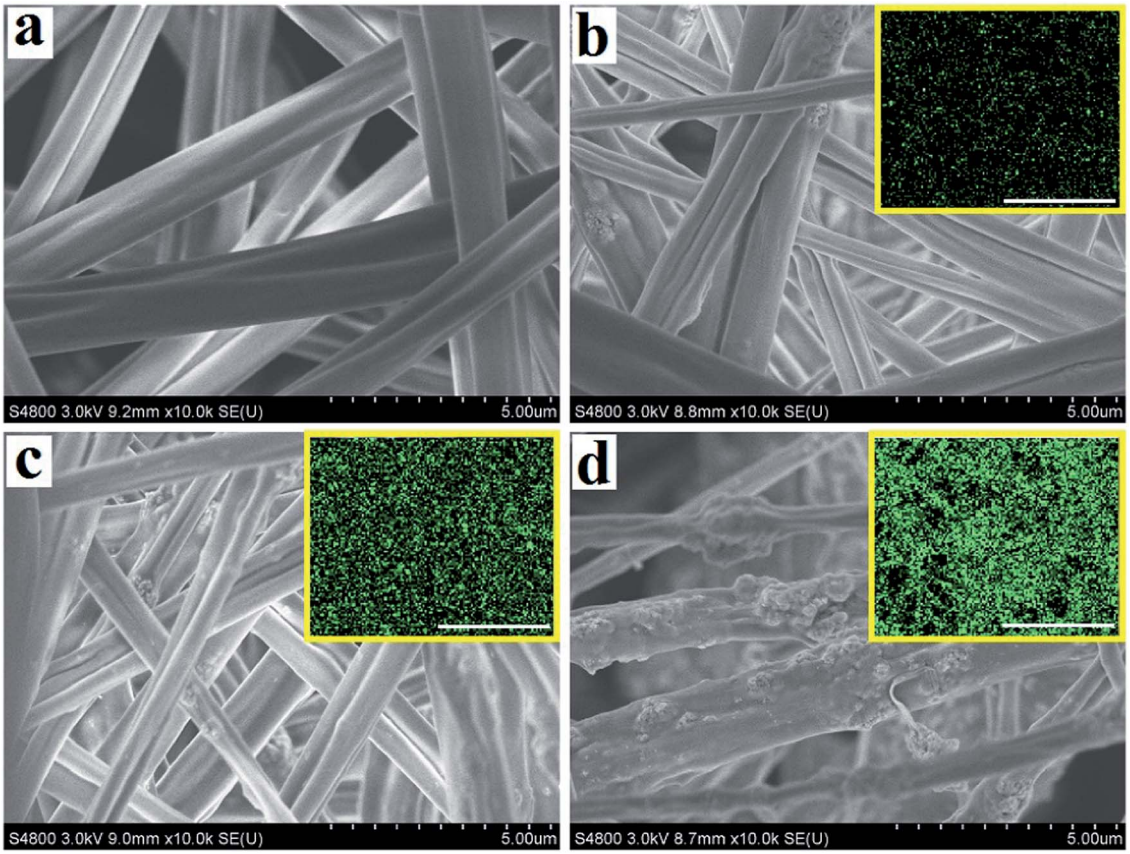

Fig. 13 SEM images and distribution of titanium element of the electrospinning CA/TiO_2 composite ultrafine fibers with various TiO_2 contents after used for MB degradation: 0 wt% (a), 1 wt% (b), 3 wt% (c), 5 wt% (d). Scare bar is 70 μm.

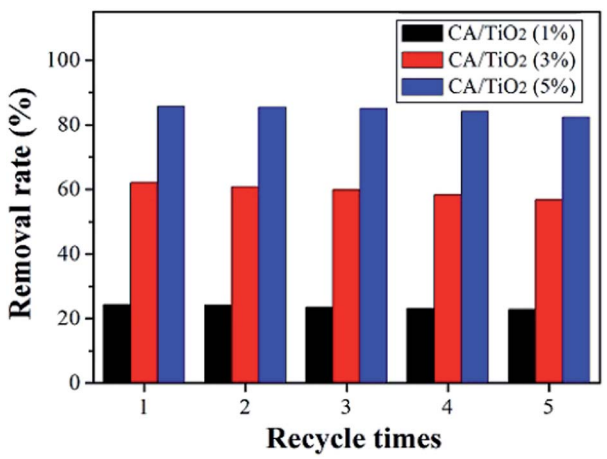

Fig. 14 Recycling test of the electrospinning CA/TiO_2 composite ultrafine fibers with various TiO_2 contents on the MB removal rate under 240 min of UV light irradiation.

the most intensive at different degradation time, which showed MB had a characteristic absorption peak at 627 nm and the intensity of the absorbance at 627 nm was proportional to the concentration of MB in the solution. Therefore, the rate of degradation reaction can be determined by measuring the intensity of the absorbance of the MB solution at 627 nm. The degradation of MB followed the first-order reaction kinetics, which can be defined as $\ln(C/C_0) = kt$, where C, C_0, k, t is the concentration after certain reaction time, initial MB concentration, the rate constant and reaction time, respectively. Fig. 11e showed the reduction rate (C/C_0) of MB containing CA composite ultrafine fibers with different TiO_2 contents under the irradiation of UV lights. It is clear that insignificant degradation of MB occurred when neat CA was irradiated with UV lights, whereas the efficiency of the TiO_2/CA composite ultrafine fibers increased variously by the deposition of different TiO_2 contents. For CA ultrafine fibers with 0, 1, 3, 5 wt% TiO_2 contents, concentration of MB reduced by about 5%, 20%, 65%, 90% respectively after 240 min degradation. From Fig. 11f, the reaction constants k for CA ultrafine fibers with 0, 1, 3, 5 wt% TiO_2 contents were calculated 0.00052, 0.00113, 0.00558 and 0.00801 min^{-1} respectively. Evidently, a higher reaction constant of the photocatalytic degradation of MB can be obtained by CA ultrafine fibers containing higher TiO_2 contents.

Fig. 12 showed photographs of CA ultrafine fibers containing different TiO_2 contents before and after used for MB degradation and color change of MB containing CA ultrafine fibers with different TiO_2 contents after 240 min degradation. Compared Fig. 12a with Fig. 12b, no obvious size changes for all samples were found after used for MB degradation except pure CA sample got blue color on it, which is due to CA's good hydrophilic property. Seen from Fig. 12c, MB dye decolored more thoroughly

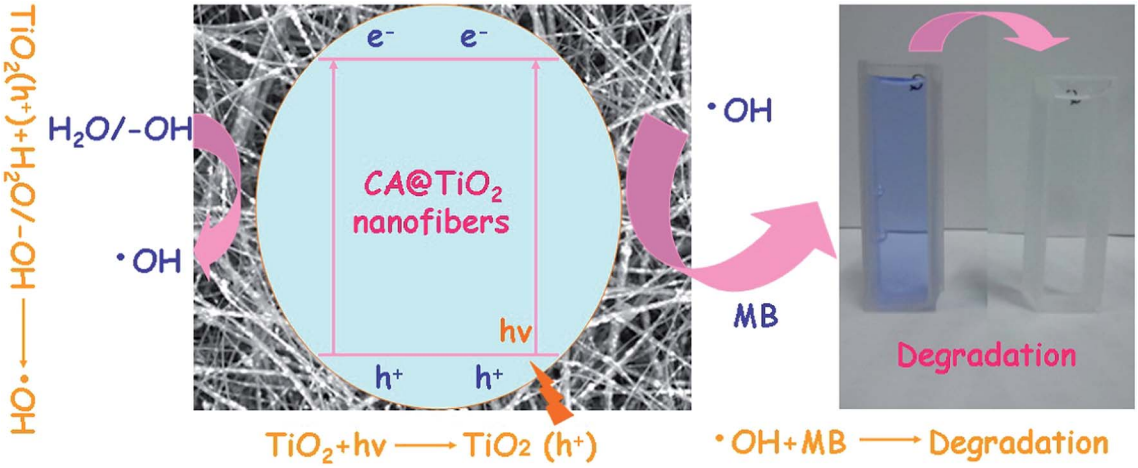

Fig. 15 A schematic illustration of photocatalytic activity of CA/TiO_2 composite ultrafine fibers.

as TiO_2 content increased, and the color changed from blue to completely transparent when its content reached 5 wt%.

Fig. 13 showed the morphology of electrospinning ultrafine fiber webs after used for MB degradation. When compared to the SEM images of the samples before used for MB degradation in Fig. 3, the morphological and fibrous structure of the CA composite ultrafine fibers after degradation were well maintained, and there was no adhesion between the fibers. Moreover, it can be seen from Fig. 13b–d that the TiO_2 NPs could be clearly observed to be deposited on/in the ultrafine fibers. Furthermore, it also can be seen form the results of EDS that titanium element distributed uniformly in the whole electrospinning membrane, indicating that the TiO_2 NPs distributed uniformly on/in the ultrafine fibers. As shown in Fig. 14, the MB removal rate of CA/TiO_2 composite ultrafine fibers with 1, 3 and 5 wt% TiO_2 NPs had only decreased a little within 5% after 5 cycles. Therefore, the as-spun CA/TiO_2 composite ultrafine fibers were confirmed to be effective for cycling use in dyeing water treatment.

For better understanding photocatalytic activity of TiO_2 NPs, the degradation mechanism of MB was illustrated in Fig. 15. As illustrated in Fig. 15, the CA/TiO_2 nanocomposite absorbed radiation of energy corresponding to its band gap and generated electron–hole pair. Then, the injected electrons might react with –OH or H_2O to form $^{\bullet}OH$ free radicals. The strong oxidative $^{\bullet}OH$ radicals along with some holes would ultimately oxidize MB and remove it from the water.

Conclusion

The CA/TiO_2 composite ultrafine fibers containing different amount of TiO_2 NPs were successfully prepared by electrospinning process. Various test instruments were utilized to characterize the fabricated composite ultrafine fibers. Catalytic activity of the composite ultrafine fibers with different TiO_2 contents was examined by a reduction reaction of MB. SEM and TEM images indicated that TiO_2 NPs had been embedded on or into the composite ultrafine fibers. Moreover, as the concentration of TiO_2 increased, the average fiber diameter of the fibers increased gradually. EDS and XRD spectrum confirmed the presence of TiO_2 NPs in the composite ultrafine fibers. XRD spectra also confirmed the tetragonal anatase structure of TiO_2 NPs. FTIR analysis showed that the introduction of TiO_2 didn't affect the hydrophilic property of CA and some interaction took place between CA and TiO_2. TG curves showed that the addition of TiO_2 improved the thermal stability of CA ultrafine fibers, and a higher thermal stability could be achieved with a higher TiO_2 content. In addition, all these analyses revealed that the incorporation percentage of TiO_2 NPs on or into the ultrafine fibers increased as its concentration increased. Photocatalytic degradation of MB showed that a higher reaction constant of the photocatalytic degradation of MB can be obtained by CA ultrafine fibers containing higher TiO_2 content. The composite ultrafine fibers were effective for cycling use in dyeing water treatment. Therefore, the CA/TiO_2 composite ultrafine fibers with good photocatalytic and natural antifouling properties, excellent recyclability and stability can be a promising, economical and environmentally friendly novel material for potential applications in dyeing water treatment.

Acknowledgements

This research was financially supported by the National Natural Science Foundation of China under grant 51073113, 91027039 and 51373110, the Natural Science Foundation of Jiangsu Province, China (no. BK20131222) and the Natural Science Foundation of the Jiangsu Higher Education Institutions of China (10KJA540046). The authors are also grateful for fund from Qinglan Project of Educational Department of Jiangsu Province (2012), the project of the Priority Academic Program Development of Jiangsu Higher Education Institutions (PAPD), Qing Lan Project for Excellent Scientific and Technological Innovation Team of Jiangsu Province (2012) and Project for Jiangsu Scientific and Technological Innovation Team (2013). This research was also financially supported by the Innovation and Entrepreneurship Leading Talent of Yancheng City (2014).

References

1 N. Azbar, T. Yonar and K. Kestioglu, *Chemosphere*, 2004, **55**, 35–43.
2 Y. R. Zhang, S. L. Shen, S. Q. Wang, J. Huang, P. Su, Q. R. Wang and B. X. Zhao, *Chem. Eng. J.*, 2014, **239**, 250–256.
3 P. Nigam, G. Armour, I. M. Banat, D. Singh and R. Marchant, *Bioresour. Technol.*, 2000, **72**, 219–226.
4 S. Ma, J. Meng, J. Li, Y. Zhang and L. Ni, *J. Membr. Sci.*, 2014, **453**, 221–229.
5 M. Z. Ge, S. H. Li, J. Y. Huang, K. Q. Zhang, S. S. Al-Deyab and Y. K. Lai, *J. Mater. Chem. A*, 2015, **3**, 3491–3499.
6 S. Y. Park, H. U. Lee, K. Ahn, J. P. Kim, J. S. Jin, J. Lee, S. Y. Jeong and C. R. Cho, *Thin Solid Films*, 2011, **519**, 6899–6902.
7 J. Chen, M. Liu, L. Zhang, J. Zhang and L. Jin, *Water Res.*, 2003, **37**, 3815–3820.
8 S. J. Doh, C. Kim, S. G. Lee, S. J. Lee and H. Kim, *J. Hazard. Mater.*, 2008, **154**, 118–127.
9 J. Yun, D. Jin, Y. S. Lee and H. I. Kim, *Mater. Lett.*, 2010, **64**, 2431–2434.
10 S. Mozia, *Sep. Purif. Technol.*, 2010, **73**, 71–91.
11 N. H. H. Hairom, A. W. Mohammad, L. Y. Ng and A. A. H. Kadhum, *Desalin. Water Treat.*, 2014, 1–12.
12 M. Ghani, A. A. Gharehaghaji, M. Arami, N. Takhtkuse and B. Rezaei, *J. Nanotechnol.*, 2014, **2**, 1–12.
13 H. J. Kim, H. R. Pant, J. H. Kim, N. J. Choi and C. S. Kim, *Ceram. Int.*, 2014, **40**, 3023–3029.
14 S. J. Kang, L. D. Tijing, B. S. Hwang, Z. Jiang, H. Y. Kim and C. S. Kim, *Ceram. Int.*, 2013, **39**, 7143–7148.
15 P. Ahmadpoor, A. S. Nateri and V. Motaghitalab, *J. Appl. Polym. Sci.*, 2013, **130**, 78–85.
16 K. Lee and S. Lee, *J. Appl. Polym. Sci.*, 2012, **124**, 4038–4046.
17 H. R. Pant, D. R. Pandeya, K. T. Nam, W. Baek, S. T. Hong and H. Y. Kim, *J. Hazard. Mater.*, 2011, **189**, 465–471.
18 C. Z. Liang, S. P. Sun, F. Y. Li, Y. K. Ong and T. S. Chung, *J. Membr. Sci.*, 2014, **469**, 306–315.
19 G. Zhang, S. Lu, L. Zhang, Q. Meng, C. Shen and J. Zhang, *J. Membr. Sci.*, 2013, **436**, 163–173.
20 S. L. Chen, X. J. Huang and Z. K. Xu, *Cellulose*, 2011, **18**, 1295–1303.
21 H. Lin, C. P. Huang, W. Li, C. Ni, S. I. Shah and Y. H. Tseng, *Appl. Catal., B*, 2006, **68**, 1–11.
22 R. Liu, H. Ye, X. Xiong and H. Liu, *Mater. Chem. Phys.*, 2010, **121**, 432–439.
23 B. Ding, E. Kimura, T. Sato, S. Fujita and S. Shiratori, *Polymer*, 2004, **45**, 1895–1902.
24 S. Sarmah and A. Kumar, *Indian J. Phys.*, 2010, **85**, 713–726.
25 T. Rojanarata, S. Plianwong, K. P. Opanasopit and T. Ngawhirunpat, *Talanta*, 2013, **115**, 208–213.
26 S. Kendouli, O. Khalfallah, N. Sobti, A. Bensouissi, A. Avci, V. Eskizeybek and S. Achour, *Mater. Sci. Semicond. Process.*, 2014, **03**, 1369–8001.
27 Y. Li, Y. Yua, L. Wua and J. Zhia, *Appl. Surf. Sci.*, 2013, **273**, 135–143.

